JACS
JOURNAL OF THE AMERICAN CHEMICAL SOCIETY

Article

pubs.acs.org/JACS

The Copper Active Site of CBM33 Polysaccharide Oxygenases

Glyn R. Hemsworth, Edward J. Taylor, Robbert Q. Kim, Rebecca C. Gregory, Sally J. Lewis, Johan P. Turkenburg, Alison Parkin, Gideon J. Davies,* and Paul H. Walton*

Department of Chemistry, University of York, Heslington, York YO10 5DD, United Kingdom

Supporting Information

ABSTRACT: The capacity of metal-dependent fungal and bacterial polysaccharide oxygenases, termed GH61 and CBM33, respectively, to potentiate the enzymatic degradation of cellulose opens new possibilities for the conversion of recalcitrant biomass to biofuels. GH61s have already been shown to be unique metalloenzymes containing an active site with a mononuclear copper ion coordinated by two histidines, one of which is an unusual τ-N-methylated N-terminal histidine. We now report the structural and spectroscopic characterization of the corresponding copper CBM33 enzymes. CBM33 binds copper with high affinity at a mononuclear site, significantly stabilizing the enzyme. X-band EPR spectroscopy of Cu(II)-CBM33 shows a mononuclear type 2 copper site with the copper ion in a distorted axial coordination sphere, into which azide will coordinate as evidenced by the concomitant formation of a new absorption band in the UV/vis spectrum at 390 nm. The enzyme's three-dimensional structure contains copper, which has been photoreduced to Cu(I) by the incident X-rays, confirmed by X-ray absorption/fluorescence studies of both aqueous solution and intact crystals of Cu-CBM33. The single copper(I) ion is ligated in a T-shaped configuration by three nitrogen atoms from two histidine side chains and the amino terminus, similar to the endogenous copper coordination geometry found in fungal GH61.

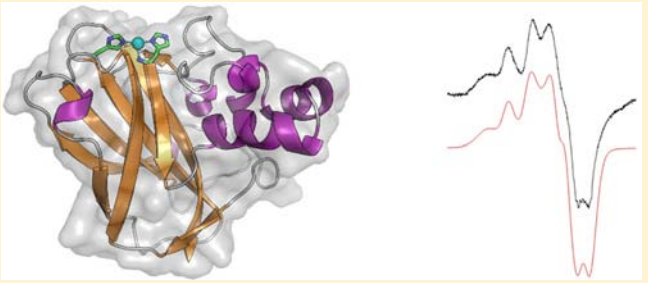

INTRODUCTION

Controlled degradation of abundant biomass is a sine qua non for the future success of bioethanol production.[1−5] In this regard, finding a means of overcoming the recalcitrance of cellulosic, lignocellulosic, or chitinotic materials either by chemical or by enzymatic methods is a major objective. Of these methods enzymatic solutions offer promise especially as recent months have seen strides toward a fuller appreciation of the consortia of ligninases, cellulases, and chitinases deployed by saprophytes and heterotrophs in the degradation of biomass.[2,6−9] In this context, an important recent advance was the discovery of a class of enzymatic oxidases, and their action on polysaccharides, reported by Harris et al.[10] and Vaaje-Kolstad et al.,[11] who demonstrated that effective fungal and bacterial depolymerization of polysaccharides hinges upon the initial action of structure-disrupting enzymes classified[12] as GH61 and CBM33, respectively. Subsequently, it was shown that GH61s from *Thermoascus aurantiacus* and *Thielavia terrestris* are new types of copper-dependent oxidases with an unusual active site, where the copper ion is bound by two histidines of the so-called histidine brace (Figure 1).[13] This finding was confirmed for fungal GH61s from *Neurospora crassa*[14,15] and *Phanerochaete chrysosporium*.[16] The active site is notable for its τ-N-methylated N-terminal histidine, the functional requirement of which is unclear. It is also similar to part of the copper active site of particulate methane monoxygenase, another powerful copper oxidase.[17]

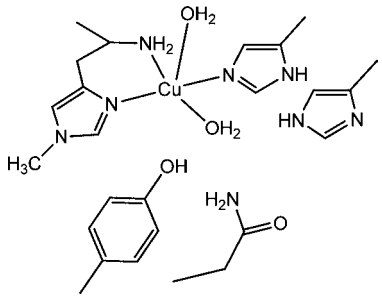

Figure 1. Active site structure of Cu(II)-GH61 showing conserved residues. Site-directed mutagenesis of the coordinated tyrosine/ate leads to reduction in activity, while mutation of glutamine leads to inactivation.[10] Cu−N(term-his) = 1.9, Cu−N(his) = 2.1, Cu−NH_2 = 2.2, Cu···O(Tyr) = 2.9 Å.

In contrast to GH61, however, and despite their potential for biofuel production, the structural and mechanistic details of CBM33 enzymes are less certain. While initial structural reports[11] suggested that Na^+, Zn^{2+}, or Mg^{2+} might be the metal at the active site, these have now been shown to be incorrect as the activity of a bacterial CBM33 from *Enterococcus faecalis*[18,19] was recently demonstrated also to be copper-dependent.

Received: October 29, 2012
Published: March 29, 2013

dx.doi.org/10.1021/ja402106e | J. Am. Chem. Soc. 2013, 135, 6069−6077

A recent NMR structure (PDB 2LHS) of a CBP21 CBM33 showed that the overall solution structure of CBP21 is similar to that of the crystallized enzyme, but while Cu perturbs the histidine NMR signals (allowing pK_a determination) showing the expected coordination of copper at the active site, no details of the copper coordination geometry could be determined from this study.[20] Also awaiting fuller elucidation is an understanding of the difference in mechanisms of action of CBM33 and GH61. For instance, analysis of the degradation products from the action of GH61 indicates oxidation at C1, C4, or C6 of the glycosidic unit, dependent on the subclass of GH61 carrying out the oxidation.[21] In these cases, GH61 action affords a linear sequence of oligosaccharide products with degrees of polymerization (dp) = 2,3,4,5,etc.[13,16,22] In contrast, where studied, CBM33 oxidation appears only to occur at C1 and affords principally oligosaccharides with dp = 2,4,6,etc.[18,23]

From a structural perspective, both enzyme classes exhibit an overall structure with a beta-sandwich core, which lies roughly perpendicular to an extended flat face, the center of which contains the active site. For GH61, substrate-binding at the face is thought to be mediated mainly by aromatic−carbohydrate interactions.[24,21] In CBM33, a lack of aromatic amino acid side chains at the binding site suggests that binding to polysaccharides is mediated through different interactions exemplified by proposals for the interaction of the "CBP21" chitin-binding CBM33.[23]

Both GH61 and CBM33 have a functional requirement for a reducing equivalent, either a sugar dehydrogenase exemplified by cellobiose dehydrogenase[14,22,25,26] or a small molecule reductant,[13] which, along with the need for dioxygen, is commensurate with a catalytic cycle in which dioxygen activation at a reduced copper site is a key step. Indeed, through further structural studies of an oxygenated form of a Cu-GH61 and in parallel with other known copper oxygenases such as peptidyl glycine monoxygenase,[27] Marletta et al. speculated on a reaction sequence for GH61 in which, following the formation of a copper(I) state and addition of dioxygen, copper(II)-superoxide is a potential oxidative species.[14,15] This proposal is based on a structure of GH61, which shows the copper ion coordinated in an axially elongated geometry, with the equatorial plane occupied by the three nitrogen atoms of the histidine brace. A water molecule occupies one axial position, and the other axial position has electron density that is assigned to a superoxide with a Cu···O distance of 2.9 Å.[28] Notwithstanding this structure, in-depth mechanistic studies are urgently required to examine not only the proposal of a copper-superoxide but also, and perhaps more importantly, whether other types of reactive copper−oxygen species could be formed as part of the reaction cycle.

As part of the continuing drive toward understanding the mechanisms of action of GH61s and CBM33s, we report here the isolation, characterization, and full three-dimensional X-ray structures of the *apo* and copper-bound forms of a CBM33 from *Bacillus amyloliquefaciens*. As initially demonstrated by Aachmann et al., we confirm that copper(II) binding to the *apo* enzyme is very tight indeed, and we further show that copper binding is accompanied by a substantial increase in protein stability.[20] Additionally, using EPR spectroscopy, we reveal details of the copper coordination sphere, which, in contrast to GH61, shows the copper ion in a coordination geometry significantly distorted from axial, such that it lies somewhat between the usual Peisach−Blumberg type 1 and type 2 classifications.[29] Three-dimensional structure and X-ray absorption spectroscopy studies of the reduced form display a copper(I) ion in a T-shaped coordination geometry, where the copper has been photoreduced by the incident X-rays.

RESULTS AND DISCUSSION

Protein Isolation, Isothermal Calorimetry, and Thermal Stability. The *Bacillus amyloliquefaciens* CBM33 domain, (first described as chitin-binding protein ChbB from a chitinolytic strain of *B. amyloliquefaciens*;[30] hereafter *Ba*CBM33), was produced from expression of the codon-optimized gene and subsequent periplasmic secretion in *E. coli* allowing processing of the signal peptide to yield the free N-terminal histidine. Standard purification with Q Sepharose and Superdex columns yielded good quantities of pure protein.

Copper(II) binding to *apo-Ba*CBM33 was followed using isothermal titration calorimetry (ITC) at 298 K, at pHs 5, 6, and 7. Copper binding has an apparent K_D of 6 nM at pH 5 (c value >1000), which is comparable to the value of 55 nM recently found for the binding of Cu(II) to CBP21.[20] Copper(II) affinity is lower at higher pH giving K_D values of 40 nM at pH 6 (c value = 325) and 80 nM at pH 7 (c = 435), with a copper to protein stoichiometry of approximately 0.8:1 (Figure 2). The small increase in K_D with pH is possibly due to

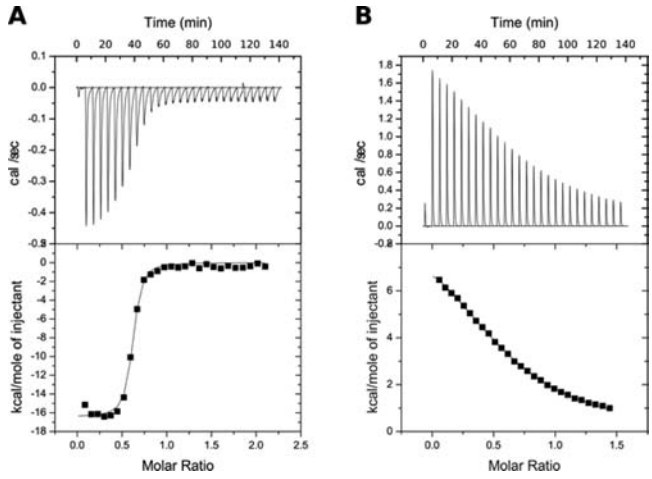

Figure 2. Isothermal calorimetry of metal binding to *Ba*CBM33: (A) Cu(II) at pH 6 (see Figure S1 for other pH measurements), (B) Zn(II) at pH 5.

competition for copper binding from the buffers used at higher pH or potentially from the deprotonation of active site residues involved in the stabilization of a metal-bound water molecule (see below for further discussion), although the reasons for these differences await a more detailed binding study. In either case, binding of copper to the enzyme is rapid and tight.

Binding of nickel(II), manganese(II), and zinc(II) at pH 5 was also investigated using ITC, with Zn(II) the only metal showing any measurable binding (Figure 2). To corroborate ITC data, the thermostability of the protein was measured in the presence of these metals. In the presence of Cu(II), the melting temperature (T_m) increased by 20 K (Figure S2), while in the presence of Ni(II) and Zn(II), a less significant shift of 7 K was observed reflecting the lower affinity of CBM33 for these metals. Mn(II) had no impact on the T_m, suggesting no binding at all. The potential binding of manganese ions was of interest because there is a single report of GH61 using Mn as a metal ion in the absence of copper.[16] However, in the case of

dx.doi.org/10.1021/ja402106e | J. Am. Chem. Soc. 2013, 135, 6069−6077

*Ba*CBM33, no Mn binding could be detected, strongly suggesting that CBM33s are uniquely copper enzymes. We also note that the enzyme does not bind further copper ions with any significant binding constant, analogous to GH61s and commensurate with the active site in CBM33s being a mononuclear copper active site, and in contrast to the dicopper site proposed for copper methane monoxygenase in which the histidine brace also appears. Such selective binding of a single copper corroborates the recent reports from activity assays that CBM33s should be classified as mononuclear copper-dependent oxygenases.[19]

Three-Dimensional Structure from X-ray Diffraction. To investigate the nature of the structure of *Ba*CBM33 in more detail and, in particular, the copper site, the three-dimensional structures of *Ba*CBM33 in *apo*, copper-bound, and copper-bound/ascorbate-soaked forms were solved by molecular replacement at resolutions of 1.8, 1.9, and 1.7 Å, respectively. The structures are analogous to those already reported for CBM33 and GH61 consisting of a core immunoglobin-like β-sandwich domain with an adjacent helical bundle (defined as loop L2 in GH61s, Figure 3).[21] As with GH61, the N-terminal

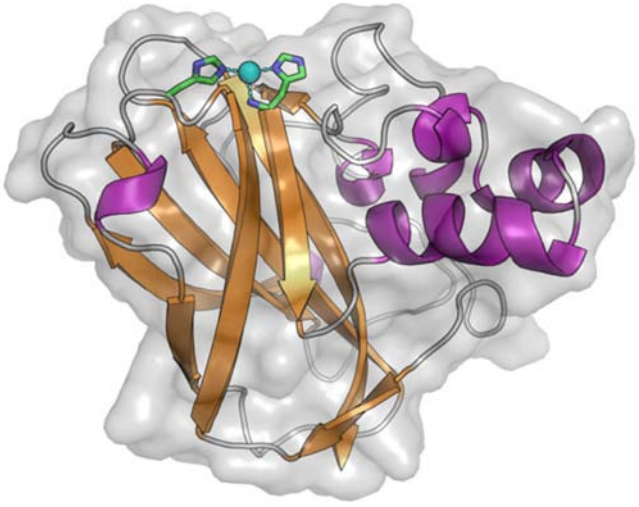

Figure 3. Structural representation of Cu-*Ba*CBM33, showing copper active site on binding face.

active site is at the center of an extended flat surface (ca. 30 × 40 Å), which is formed by the helical bundle and the narrow end of the β-sandwich. This surface presumably interacts in a face-to-face manner with the surface of the substrate, bringing the copper into close contact with the polysaccharide.

Structural variation between the active sites of the *apo* and both copper-bound forms is minimal, revealing a degree of preorganization for copper binding (Figure S3), consistent with the high copper-binding affinity. In the copper-bound form at the N-terminal histidine active site, well-defined electron density consistent with a single, fully occupied copper ion was found, coordinated in a T-shaped configuration of the histidine brace by the nitrogen atoms of two histidine side chains and the amino terminus [$\angle N_{his}-Cu-NH_2$ = 96° and $\angle NH_2-Cu-N_{his}$ = 98°], with $Cu-N_{his}$ distances of 2.0 and 2.0 Å and a longer Cu−N (amino terminus) distance of 2.3 Å (Figure 4). Unlike GH61, there is no tyrosine/ate present in the apical position of the coordination sphere, which is replaced by a phenylalanine in CBM33. Additionally, in contrast to GH61, the N-terminal histidine is not τ-N-methylated. These

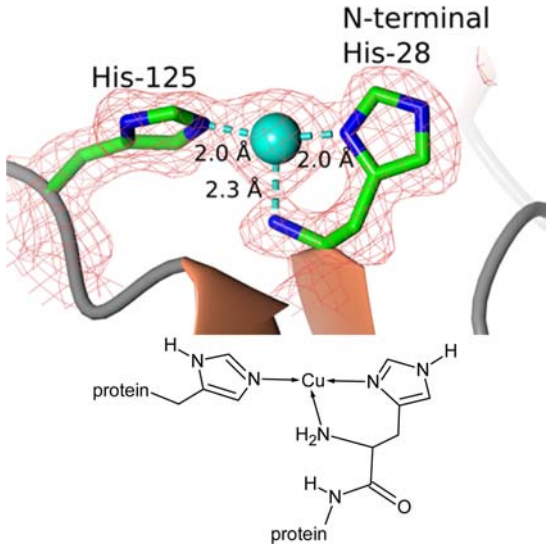

Figure 4. Top: Electron density map contoured at 1σ in the active site of Cu-*Ba*CBM33; see Figure S4 for stereo view. Bottom: Line diagram of active site; cf., Figure 1 for comparison to active site of GH61.

differences, if indeed present in the wild-type enzyme, would amount to a significant variance in the active site electronics of the copper site in CBM33 and point toward differing mechanisms of action between the two enzymes, possibly dictated by the oxidation requirements of different natural substrates.

Surprisingly, no further significant electron density (>0.3 σ) was found in the primary coordination sphere of the putative copper(II) ion, inconsistent with the dearth of known small molecule T-shaped copper(II) complexes. Indeed, only one genuine copper(II) complex in a N_3 T-shaped geometry is known, and in this complex the EPR spin Hamiltonian values are markedly different from those of Cu(II)-*Ba*CBM33 (see below for further discussion).[31,32] The T-shaped coordination geometry in the structure of Cu-*Ba*CBM33 is, however, consistent with a copper(I) formulation, especially because there is no difference in copper coordination sphere when the crystals are soaked with sodium ascorbate and the structure redetermined. The possibility of a reduced copper oxidation state is corroborated by small molecule studies of copper-bis(pyrazolyl) amine ligands, where the nitrogen atoms of the ligand occupy a T-shaped configuration, and studies of three coordinate copper in histidylhistidine complexes, both of which also have high redox potentials.[33,34]

X-ray Absorption Spectroscopy Studies of Copper Oxidation State. To confirm the presence of copper(I) in the structures, we performed a Cu K-edge XANES study both of the in situ crystal during diffraction data collection and of an aqueous solution of Cu(II)*Ba*CBM33 at pH 5 both before and after exposure to synchrotron X-rays (Figure 5). X-ray exposure of a 0.6 mM solution of Cu(II)-*Ba*CBM33 at pH 5 led to the rapid (after a single scan) formation of a pre-edge feature at 8982−3 eV. This feature could also be generated from the addition of a solution of reducing agent (sodium ascorbate at pH 5), which is further known to afford an EPR silent species. The XANES absorption at 8983 eV is assigned to a 1s to nonbonded 4p transition of a coordinatively unsaturated copper(I) ion; this transition is a reliable marker of copper oxidation state and also of low (<4) coordination number.[34−37] Moreover, in this case, the profile of the pre-edge region

dx.doi.org/10.1021/ja402106e | *J. Am. Chem. Soc.* 2013, 135, 6069−6077

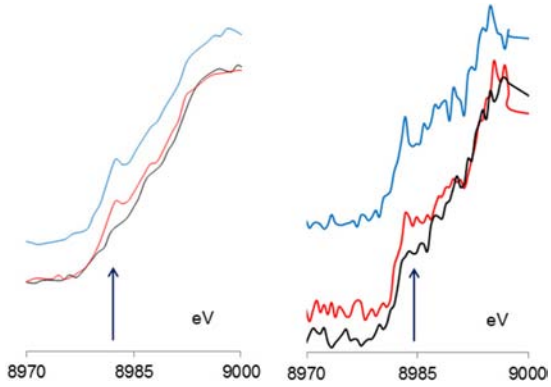

Figure 5. Left: 0.6 mM Cu-*Ba*CBM33 solution at pH 5 (1 eV steps). Right: In crystallo (0.5 eV steps), successive Cu K-edge XANES fluorescence spectra (black line followed by red line) showing growth of pre-edge peak at 8982−3 eV. Blue spectrum (offset in ordinate for clarity) is that of Cu-*Ba*CBM33 solution/crystal pretreated with sodium ascorbate solution.

matches closely to that of a known small molecule copper(I) complex in which the copper ion is coordinated in T-shaped configuration formed by two trans pyrazolyls and one bridgehead amine,[38,39] directly analogous to the observed copper structure in Cu-*Ba*CBM33.

To link the crystallographic and solution phase studies, we performed fluorescence XANES studies of the in situ crystal. Notwithstanding their relatively low signal-to-noise, these spectra display the same pre-edge feature and behavior as that observed in solution. We therefore infer that the *Ba*CBM33 copper-bound structure is of the copper(I) form, where the copper ion has been unavoidably photoreduced by the X-rays. This observation underlines the need for very considerable caution in the interpretation of oxidation state and coordination geometry in the X-ray structures of copper enzymes that contain the copper histidine brace structure, a point convincingly made some years ago by Somerhalter et al.[40] and a feature of the early structures of CBM33 and GH61, which goes some way to explain the confusion about the identity of the metal ion.[10,11]

Redox Studies of Cu*Ba*CBM33. The ostensibly high redox potential of Cu*Ba*CBM33 implied from the XAS studies was investigated using the method of titration of Cu(II)-*Ba*CBM33 against a range of redox-active dyes with known redox potentials, indicating a redox potential for Cu*Ba*CBM33 of between ∼275 and 370 mV (Figure S7). Recent studies of a Cu-CBP21 yielded a comparable value of the redox couple of ca. 275 mV at pH 6 (vs SHE).[20]

The relatively high potential is expected from the low coordination number of the copper ion in CBM33. This has also been observed in studies of copper histidylhistidine complexes.[34] Furthermore, low coordinate copper(I) centers have been proposed to be the sites of reactive-oxygen-species (ROS) production in copper amyloid-β fragments.[36] In both cases, the redox potential of the copper(I) complex and its reactivity toward dioxygen is critically dependent on the balance of three coordinate versus two coordinate copper(I), which, in the context of GH61 and CBM33, implies a significant role in oxygen activation for the central amino terminus in the coordination sphere of the copper ion. Additionally, the principal ROS product in copper amyloid-β fragments appears to be peroxide rather than superoxide, requiring the presence of a redox-active tyrosine/ate within the peptide fragment. A similar situation could occur within GH61 and CBM33, both of which have conserved tyrosines or tryptophans within their sequences (see below).[19,21]

X-Band EPR Spectroscopy of *met*-Cu*Ba*CBM33 and Azide Binding Studies. In the absence of structural information from X-ray crystallography, the nature of the copper(II) site in Cu(II)-*Ba*CBM33 was investigated using frozen solution X-band EPR spectroscopy at 155 K. Cu(II)-*Ba*CBM33 exhibits a rhombic spectral envelope ($g_x \neq g_y \neq g_z$) but where the SOMO has significant d(x^2-y^2) character, indicating a mononuclear copper(II) ion in a single binding site (Figure 6) with distorted-axial coordination geometry.

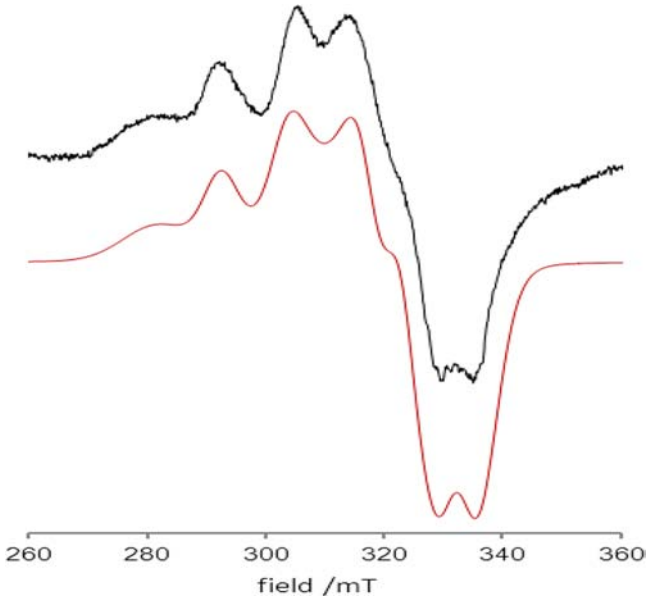

Figure 6. X-Band (9 GHz, 155 K) EPR spectrum (top) with simulation in red (bottom) of Cu(II)*Ba*CBM33 at pH 5 (15% v/v glycerol).

Simulation of the spectrum was hampered by the second-order nature of the perpendicular region, making a determination of the g_x and g_y and $|A_x|$ and $|A_y|$ tensor values unreliable. Spin Hamiltonian tensor values in the parallel direction, however, could be modeled accurately with g_z = 2.25 and $|A_z|$ = 125 G (0.0135 cm^{-1}). These values place Cu(II)-*Ba*CBM33 between the usual Peisach−Blumberg classifications of type 1 and type 2 copper enzymes, although the overall axial envelope of the EPR signal would suggest that a type 2 classification is appropriate.[29] The somewhat low $|A_z|$ value in combination with low g_z could arise from increased metal−ligand covalency or, more likely given the rhombicity of the spectrum and the potential absence of ligands on the *z*-axis (see structure discussion below), a coordination geometry at the copper that is distorted away from a local axial symmetry, possibly by the coordination of one or two water molecules, neither of which is directly trans to the amino terminus. This distortion allows the SOMO to mix with 3d(z^2) and/or 4s orbitals, affording a greater relative contribution of spin-dipolar and/or Fermi contact terms to the hyperfine coupling.[41,42] Additional evidence for a distorted coordination geometry comes from noting the similarity of the g_z and $|A_z|$ values for Cu(II)-*Ba*CBM33 with those of the copper site in Cu−Zn superoxide dismutase, in which the copper has a distorted square planar coordination geometry.[43] Furthermore, an existing X-ray

dx.doi.org/10.1021/ja402106e | *J. Am. Chem. Soc.* 2013, 135, 6069−6077

structure of a CBP21, which, despite the incorrect assignment of the metal ion as Na^+ at the active site (PDB entry 2BEM), exhibits a distorted square planar coordination at the metal where the three nitrogen atoms of the histidine brace and the metal ion occupy a plane and where a water molecule in the fourth coordination site is significantly deviated from this plane.[11]

Addition of sodium azide to a solution of Cu(II)*Ba*CBM33 at pH 5 affords changes in both UV/vis and EPR spectra. In the latter, addition of stoichiometric azide gives a shift in g_z to 2.23 and $|A_z|$ to 0.0125 cm^{-1}, but no change in the overall spectral envelope. Addition of a 10-fold excess of azide affords a significant change with the formation of new peaks but with loss of some of the fine structure (Figure S5), indicative of coordination to the copper(II) center. In the UV/vis spectrum, a single intense band (ca. 900 dm^3 mol^{-1} cm^{-1}) appears at ~390 nm assignable to an azide to copper charge transfer band at a mononuclear copper site.[44] The appearance of this band is accompanied by a small increase in the intensity of the d−d transition absorption of the Cu(II) center at ca. 690 nm (Figure 6).

There are distinct differences in the EPR spectrum of Cu(II)-*Ba*CBM33 and that of Cu(II)-*Ta*GH61. In the latter, the g_z and $|A_z|$ values of 2.27 and 0.0162 cm^{-1} place GH61 squarely within the type 2 classification of copper site and are also indicative of a copper(II) ion within an axial coordination geometry. This geometry was confirmed by the subsequent X-ray diffraction studies of GH61. It is currently unclear why there are such differences in the coordination geometries of the *met* forms of both CBM33 and GH61, but the difference is likely to be of functional significance given the differences in the copper active site structures of CBM33 and GH61 (see below).

Sequence Conservation Analysis of CBM33s and Comparison to CBP21 and GH61s. An amino acid sequence alignment of *Ba*CBM33 with a range of selected CBM33s is shown in Figure S6. Outside the active site histidines, strict conservation is observed in parts of the β-sandwich and in a collection of tryptophan residues adjacent to the active site, where the latter is probably associated with an electron transfer function. This particular conservation of tryptophans is also observed in CBP21 chitin oxidases, as previously noted by Vaaje-Kolstad et al.[19]

An unusual feature in CBM33 is observed in the strict conservation of an alanine residue at position 123 at the end of a β strand. The methyl group of this alanine is close to the apical coordination site on the copper ion (Cu···C = 3.9 Å), thereby providing a degree of steric congestion at this coordination site. What makes this feature notable is that the opposite apical site is occupied by a highly conserved phenylalanine side chain (position 196), which has a near "end-on" aspect to the copper ion with a closest Cu···C distance of 3.7 Å (Figure 7). The combination of the alanine and phenylalanine suggests that coordination to the copper in CBM33 is restricted to equatorial sites only (Figure 7). This is in sharp contrast to GH61 where the apical sites are occupied by the oxygen atoms of a tyrosine/ate and a water molecule, where the water molecule could be replaced by either substrate or an oxygen molecule, as suggested by Li et al.[21] Whatever the reasons for the differences between CBM33 and GH61, the contrasting arrangement of amino acid side chains in the copper ions' secondary coordination spheres, including that of the τ-N-methylated N-terminal histidine in GH61, is indicative of different mechanisms of action between the two enzymes.

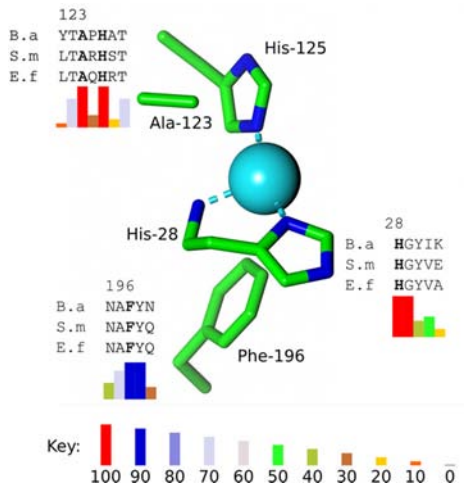

Figure 7. Active site conserved residues in CBM33 depicting the occlusion of Cu(II) axial coordination sites by alanine 123 and phenylalanine 196. Sections of the sequence alignment with two other CBM33s (B.a = *Bacillus amyloliquefaciens*, S.m = *Serratia marcescens*, and E.f = *Enterococcus faecalis*)[19,23] are shown surrounding each of the active site residues, which are shown in bold. Their associated percentage identities from the full sequence alignment shown in Figure S6 are indicated by the histograms below the sequences according to the key.

In a further indication of alternative mechanisms, the conserved residues on the binding face of CBM33 differ from that of GH61s. In the former, the principal conservation pattern is found in amino acid side chains, which can engage in hydrogen-bond interactions with a polysaccharide substrate. These residues lie in two areas immediately adjacent to the copper active site. The two regions lie on opposite sides of the copper ion, thus providing an environment that likely directs a specific orientation of the substrate with respect to the copper and thus any reactive oxygen species generated at the active site. Such a directed interaction with the substrate is in accordance with the observation that CBM33s react principally at the C1 site of β-linked polysaccharides; it may also offer an explanation as to why only even-numbered oligosaccharides are produced by CBM33 insofar as the up−down−up−down orientation pattern of individual glycoside units within chitin and cellulose will only project C−H bonds (from C−1) toward the enzyme binding face every other glycosidic unit, as first suggested by Vaaje-Kolstad et al.[19,23]

GH61s appear to bind to substrate through multiple aromatic−carbohydrate interactions. This was shown by Li et al., who identified conserved tyrosine residues on the α-helical L2 loop in polysaccharide oxygenases and also on residues near the copper active site (Figure 8).[21] The residues are not only in different positions on the binding face when compared to CBM33s, but also probably interact with the cellulose substrate in a somewhat less directional way than the potential hydrogen-bonding interactions seen in CBM33. This is commensurate with a wider range of oxidation sites on cellulose that is observed with GH61 oxidative action, especially type 3 PMOs,[21] and that oxidation does not only occur at the exposed C1−H bonds on cellulose, as appears to be the case in CBM33.

It is not possible to be more definitive about the conservation differences between CBM33 and GH61 because we are unable to rule out the possibility of post-translational modifications on

dx.doi.org/10.1021/ja402106e | J. Am. Chem. Soc. 2013, 135, 6069−6077

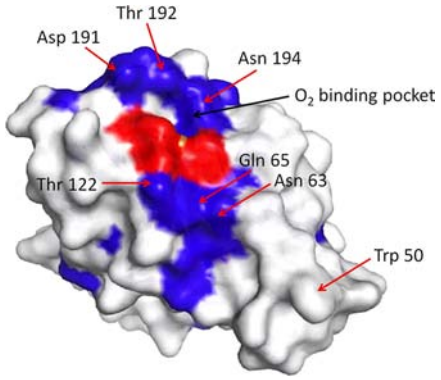

Figure 8. Binding face of *Ba*CBM33 indicating conserved residues. Region colored red is copper active site, which is surrounded by highly conserved regions consisting of residues capable of forming hydrogen bonds with substrate. L2 loop region is to bottom right of figure, showing no noticeable conservation, in contrast to type 2 PMOs (GH61s), which exhibit conservation of some aromatic residues.[21]

CBM33, which could introduce extra functionality at the active site, for instance, oxidation of phenylalanine to tyrosine and potential methylation of the N-terminal histidine. Indeed, we observe here that one CBM33 sequence naturally has a tyrosine in place of phenylalanine 196. Nor can we completely rule out a coordinative role for a highly conserved tyrosine at position 197, although note that this appears to be unlikely given the large structural disruption this would entail and the absence of any conformational flexibility in this region as observed across several sets of deposited coordinates. Additionally, an interrogation of the CAZy database shows that GH61s can appear as multidomain proteins in which the oxygenase domain is fused to other known cellulose-binding modules (e.g., CBM1) through which binding to cellulose will be significantly affected.[45] Similarly, CBM33 enzymes are often appended to diverse other protein modules involved in hydrolysis and binding of carbohydrates, as reviewed recently by Horn et al.[4] Notwithstanding these caveats, however, a structural basis for the known differences in mechanisms of action of CBM33s and GH61s does emerge without the need to introduce significant post-translational modifications in CBM33s, and may well therefore be a reliable basis for understanding differences in reactivity.

■ CONCLUSIONS

We have demonstrated that a CBM33 from *Bacillus amyloliquefaciens* binds copper(II) with a $K_d \approx 6$ nM. This binding significantly stabilizes the enzyme, probably reflecting the increased formation of a folded state of the protein backbone. From X-band EPR spectroscopy and azide binding studies, we can infer that Cu-*Ba*CBM33 is a mononuclear type 2 copper enzyme, but where the copper(II) ion has a distorted axial geometry, possibly a distorted square planar configuration akin to that seen in structure of Cu−Zn superoxide dismutase. XANES spectroscopy demonstrates that the copper is susceptible to reduction and is readily photoreduced by X-rays both in solution and in the solid state to the copper(I) form, an observation supported by the high redox potential of Cu-*Ba*CBM33. (Very recently, structures of a CBM33 from *Enterococcus faecalis* were released on the pdb, the deposition titles of which imply a similar photoreduction of copper when coordinated by the histidine brace; pdb codes: 4alr, 4als, 4alt, 4alq, 4ale, 4alc. Currently, no further publication accompanies the release of these coordinates.) Single-crystal X-ray diffraction shows that the enzyme adopts an active site structure, which has broad parallels with that reported for Cu-GH61s. The copper(I) histidine brace coordination geometry in Cu-*Ba*CBM33 is T-shaped N_3, corroborated by XANES studies that show a 1s to nonbonded 4p transition characteristic of low coordination number copper(I) species. Differences in the secondary coordination sphere of the copper ion in CBM33s and GH61s are suggestive of a different mechanism of action in the two classes of enzymes, but a fuller understanding of the mechanism awaits in-depth and detailed reaction studies on the enzymes and their associated small molecule model complexes.

■ EXPERIMENTAL PROCEDURES

Expression and Purification of BaCBM33. The coding sequence of *Bacillus amyloliquefaciens* CBM33 (NCBI Reference Sequence: NC_014551.1) from nucleotide 82 to 621 was codon optimized for expression in *Escherichia coli*, synthesized with a pelB leader sequence to direct the protein to the periplasm, and cloned into the pET-11a vector, by GenScript. The resulting pET11a-BaCBM33 construct was used to transform BL21 (DE3) *E. coli*, which were grown from a single colony in six 500 mL LB cultures to an A_{600} of 0.4 at 37 °C shaking at 180 rpm. The temperature was then reduced to 16 °C, and the cells were allowed to grow further to an A_{600} of 0.6−0.8 when expression was induced by the addition of IPTG to a final concentration of 1 mM. The cultures were left overnight before the cells were harvested by centrifugation at 11 000*g* for 30 min at 4 °C.

Cells were immediately resuspended in 5 volumes of ice cold resuspension buffer (50 mM Tris pH 8.0, 200 mM NaCl, 20% w/v sucrose). To isolate the periplasmic fraction, 40 μg of hen egg white lysozyme (Sigma-Aldrich) was added for every gram of cell paste and left on ice for 1 h. 60 μL of 1 M $MgSO_4$ was then added per gram of cell paste, and the suspension was incubated for a further 20 min on ice. Cell debris was then removed by centrifugation at 10 000*g*, 4 °C for 10 min, and the supernatant containing the periplasmic fraction was removed into a fresh tube. This was diluted 4 fold with buffer A (50 mM Tris pH 8.0) and passed through a 5 mL HiTrap Q Sepharose column equilibrated in the same buffer collecting the flow through. The column was then stripped with 100% buffer B (50 mM Tris pH 8.0, 2 M NaCl). BaCBM33 did not bind to the column and was present in the flow through, which was precipitated by the addition of solid ammonium sulfate to a final concentration of 3.5 M and left stirring overnight at 4 °C. The protein was then isolated by centrifugation at 38 000*g* for 30 min, the supernatant was discarded, and the pellet was dissolved in 10 volumes of buffer C (20 mM sodium acetate pH 5.0, 250 mM NaCl, 5 mM EDTA). The protein was then concentrated to less than 10 mL and applied to a HiLoad 26/60 Superdex 75 column equilibrated in GF buffer (20 mM sodium acetate pH 5.0, 250 mM NaCl). Peak fractions containing pure BaCBM33 were pooled and concentrated using a Sartorius 10 kDa cut off concentrator at 4000*g*. Protein concentrations for all subsequent experiments were determined by measuring the A_{280} using an extinction coefficient of 44 920 M^{-1} cm^{-1} and a molecular weight of 19 821 Da.

Redox Potential Measurements. The redox indicator dyes thionine, tetramethylphenylenediamine (TMP), and 2,6-dichlorophenolindophenol (DCPIP) were purchased from Sigma. A three-electrode setup was used to determine accurately the reduction potential of the redox indicators and potassium ferricyanide in 100 mM sodium acetate buffer, pH 5. A stationary Pt disc working electrode (BASi), a Pt wire counter electrode, and a saturated calomel reference electrode (SLS) were all placed into an all-glass electrochemical cell. Cyclic voltammograms (50 mV s^{-1}) were measured for 1 mM solutions of each of the redox compounds under a flow of Ar. A correction factor of $E_{SHE} = E_{SCE} + 0.241$ V was used. The resultant scans are shown in Figure S7. The anodic and cathodic peak potentials, as determined by the electrochemical software (Epsilon BASi), were averaged to give the midpoint reduction potentials, summarized in

dx.doi.org/10.1021/ja402106e | *J. Am. Chem. Soc.* 2013, 135, 6069−6077

Table S2. To judge if the dye could reduce *Ba*CBM33, up to 10 μL of approximately 0.5 mM enzyme was injected into a suba-sealed cuvette containing 150 μL of reduced dye solution (absorbance <0.2 AU) and a small stirrer bar. Following 2 min of stirring, any resulting color changes were monitored using UV−vis spectroscopy. Control experiments were conducted with injection of buffer instead of enzyme, and it was confirmed that CBM33 was required to oxidize thionine or TMP in the cuvette.

EPR Spectroscopy. Continuous wave X-band frozen solution EPR spectra of 0.5 mM solution of Cu(II)-BaCBM33 (15% v/v glycerol) at pH 5 (acetate buffer) and 155 K were acquired on a Bruker ESP 300 spectrometer operating at 9.072 or 9.35 GHz, with a modulation amplitude of 4G and microwave power of 5 mW. Spectra were referenced against DPPH. Spectral simulation was carried out using Easyspin 4.0.0 on a desktop PC. Simulation parameters were as follows: g_x = 2.075, g_y = 2.086, g_z = 2.255; $|A_x|$ = 39, $|A_y|$ = 90, $|A_z|$ = 125 G. Strain: A_{xx} = 210, A_{yy} = 210, A_{zz} = 210 G. Linewidth: 40 G (Gaussian), 40 G (Lorentzian). g_z and $|A_z|$ were determined accurately from the two absorptions at low field where it was assumed that these absorptions were separated from other aspects of the absorption envelope. It was assumed that *g* and *A* tensors were axially coincident. Accurate determination of the g_x, g_y, $|A_x|$, and $|A_y|$ was not possible due to the second-order nature of the perpendicular region and the significant level of conformational heterogeneity, although it was noted that satisfactory simulation could only be achieved with one particular set of spin Hamiltonian values.

Solution XANES Spectroscopy. XANES spectroscopy data were collected on a 0.6 mM solution of Cu(II)-BaCBM33 at pH 5, which had been flash-frozen to 77 K (0.7 mM BaCBM33 was prepared in 20 mM sodium acetate pH 5.0, 250 mM NaCl to which $Cu(NO_3)_2{\cdot}3H_2O$ was added to a final concentration of 0.6 mM; to produce a Cu(I) sample, ascorbate was added to a final concentration of 10 mM). Data were acquired on the sample at 90 K at the B18 Core Spectroscopy beamline at Diamond Light Source, Oxfordshire, UK. At the time of the measurement, the Diamond synchrotron was operating at a ring energy of 3 GeV in a 10 min top-up mode for a ring current of 301 mA. The beamline was equipped with a Si(111) double crystal monochromator, and harmonic rejection was achieved through the use of two Pt-coated mirrors operating at an incidence angle of 9 mrad. The monochromator was calibrated using the first maximum in the derivative in the edge region of the XAS spectra of a copper foil placed between the second and third ion chambers at 8979 eV. Estimated flux of beam at 8 keV = 5×10^{11} ph/s. Data were collected in fluorescence from 8779 to 9020 eV using a nine-channel Ge solid-state detector at the copper K absorption edge (~8980 eV) in 1 eV steps. The sample was contained in a 5 mm light path PTFE 400 μL cell with 25 μm thick windows made from Kapton foil. The measurements were made at 90 K. The incident beam intensity was measured using a 30 cm ion chamber optimized using a helium−nitrogen gas mixture to absorb 30% and 70% of the beam in I0, respectively.

XANES Data Collection in the Crystal. X-ray fluorescence scans were performed on crystals, which had not previously been exposed to X-rays on station I03 of Diamond Light Source, using a Vortex multicathode, single element detector. Crystals from copper cocrystallizations, as grown for the structure determination, were washed through three drops of cryo-protectant solution to remove excess copper prior to plunging in liquid nitrogen. To produce Cu(I) control samples, 20 mM ascorbate was included in the cryo-protectant soaking solution. Fluorescence scans were performed across the copper K-edge from 8942 to 9017 eV with step sizes of 5 eV from 8942 to 8962 eV, 0.5 eV across the edge from 8962 to 8997 eV, and 5 eV from 8997 to 9017 eV.

Isothermal Titration Calorimetry. Isothermal titration calorimetry was performed using a VP-ITC calorimeter (MicroCal). Typically protein was present in the cell between 10 and 120 μM with a 10-fold more concentrated solution of $CuCl_2$ in the syringe. Titrations were initially performed at 283 K, but the same results could later be obtained at 298 K also. After an initial 2 μL injection, which is discarded in the data analysis, 10 μL injections were used during the titration with a 5 min interval between each injection at pH 5.0 and 6.0 and 8 min intervals at pH 7.0 where binding was slower. The buffers used during the titrations were either 20 mM sodium acetate pH 5.0, 250 mM NaCl, 20 mM Bis-Tris pH 6.0, 250 mM NaCl, or 20 mM Bis-Tris pH 7.0, 250 mM NaCl with the $CuCl_2$ solution prepared in exactly the same buffer. All data were analyzed using the Origin 7 software package (MicroCal). Heats of dilution were subtracted from the data, but the analysis routinely returned a substoichiometric binding of Cu. Modification of the injection system to remove Cu-containing brass components improved the stoichiometries, but these rarely exceeded 0.86. This is likely due to a portion of the protein having acquired Cu^{2+} given the very high affinity of the interaction from the glassware. To give meaningful ΔH values (the K_Ds are unaffected), the protein concentration was therefore adjusted in the software to reflect the 1:1 stoichiometry of copper to protein seen in the crystal structure.

Differential Scanning Fluorimetry. Differential scanning fluorimetry was used to determine the melting temperature of *Ba*CBM33 with and without metal ions. Stability measurements were performed using an Agilent MX3000P QPCR machine and the fluorescent dye SYPRO orange (Sigma-Aldrich) diluted 2000 fold from the stock solution. Fluorescence was measured with excitation and emission wavelengths of 517 and 585 nm, respectively. All experiments were performed in 20 mM sodium acetate pH 5, 250 mM NaCl with protein at 25 μM, and a total volume of 30 μL. Fluorescence was monitored while increasing the temperature in steps of 1 °C at 30 s intervals from 25 to 96 °C. The fluorescence was significantly quenched in the presence of copper, but a melting curve could still be obtained. Melting temperatures (T_m) were calculated by fitting a sigmoidal curve to the data using the MTSA[46] program for MATLAB.

Crystallization of *Apo* and Cu-Bound BaCBM33. To form the Cu complex, $Cu(NO_3)_2{\cdot}3H_2O$ was added to the protein to a final concentration of 1 mM. *Apo* and Cu cocrystallization trials were then set up in parallel with a protein concentration of 7 mg/mL using a Mosquito robot (TTP Labtech). The best crystals in both cases were obtained in condition D1 of the PACT screen (Qiagen): 0.1 M MMT buffer pH 4.0, 25% PEG-1500. Crystals were used directly from these initial screens for subsequent data collection. Crystals used to determine the Cu-bound/ascorbate soaked structure were cocrystallized with copper in the same way as described above.

Diffraction Data Collection, Processing, and Structure Determination. Crystals were cryo-cooled for data collection by first soaking for 30 s in mother liquor supplemented with 20% v/v ethylene glycol before plunging directly in liquid nitrogen. For the ascorbate soak, 20 mM sodium ascorbate was included in the cryo-protectant. Diffraction data were collected at Diamond Light Source, beamlines I04-1 and I03 at wavelengths of 0.917 and 0.976 Å, respectively. Data were indexed and integrated using XDS[47] with subsequent processing performed using the CCP4 software package.[48] The *Serratia marcescens* CBP21 structure (pdb 2ben)[49] was prepared as a molecular replacement search model using CHAINSAW,[50] cutting back side chains to their nearest common atom. The *Apo* and Cu-bound structures were initially determined by molecular replacement using PHASER,[51] both containing two molecules in the asymmetric unit. Following structure solution, pseudotranslational symmetry was detected in the *apo-Ba*CBM33 data. The structure was therefore solved again using MOLREP inputting the pseudo translation vector 0.500, 0.000, 0.127 for the off-origin Patterson peak. ARPwARP[52] was then used to rebuild the initial models before subsequent manual building and refinement using COOT[53] and REFMAC5,[54] respectively. Local NCS restraints were applied using the automatic NCS option in REFMAC5. The ascorbate soaked crystals were isomorphous to the copper-free crystals, and so the copper-free structure was simply refined against these data, with waters and flexible loops removed, to yield the structure. This was rebuilt and refined with COOT and REFMAC5 as for the others. All data processing and refinement statistics can be found in Table S1. Coordinates and accompanying structure factors for the *apo*-, Cu-bound, and Cu-bound/ascorbate soaked enzyme have been deposited in the protein data bank with accession codes 2YOW, 2YOX, and 2YOY, respectively.

■ ASSOCIATED CONTENT

Supporting Information

Experimental details, additional experimental data, EPR simulation data, sequence identity analysis, and redox measurement methods. This material is available free of charge via the Internet at http://pubs.acs.org.

■ AUTHOR INFORMATION

Corresponding Author

paul.walton@york.ac.uk; gideon.davies@york.ac.uk

Notes

The authors declare no competing financial interest.

■ ACKNOWLEDGMENTS

We thank Dr. Victor Chechik for EPR assistance and Lorna Clark and James Robinson for laboratory support. G.R.H. is funded by the BBSRC under grant BB/I014802/1. G.J.D. thanks the Royal Society for the provision of a Wolfson merit award. E.J.T. gratefully acknowledges the Royal Society for the provision of a University Research Fellowship. We thank Diamond Light Source stations I03, I04-1, and B18 for provision of X-ray facilities.

■ REFERENCES

(1) Douglas, B. J.; Michael, J. B.; Jay, D. B.; Bruce, S.; Ronald, E. H.; Charles, C. L.; Jeffrey, A. M.; Kurt, W. *Biochem. J.* **2012**, *442*, 241.

(2) Sweeney, M. D.; Xu, F. *Catalysts* **2012**, *2*, 244.

(3) Viikari, L.; Vehmaanperä, J.; Koivula, A. *Biomass Bioenergy* **2012**, *46*, 13.

(4) Horn, S. J.; Vaaje-Kolstad, G.; Westereng, B.; Eijsink, V. G. H. *Biotechnol. Biofuels* **2012**, *5*, 45.

(5) Gelfand, I.; Sahajpal, R.; Zhang, X.; Izaurralde, R. C.; Gross, K. L.; Robertson, G. P. *Nature* **2013**, *493*, 514.

(6) Floudas, D.; Binder, M.; Riley, R.; Barry, K.; Blanchette, R. A.; Henrissat, B.; Martínez, A. T.; Otillar, R.; Spatafora, J. W.; Yadav, J. S.; Aerts, A.; Benoit, I.; Boyd, A.; Carlson, A.; Copeland, A.; Coutinho, P. M.; de Vries, R. P.; Ferreira, P.; Findley, K.; Foster, B.; Gaskell, J.; Glotzer, D.; Górecki, P.; Heitman, J.; Hesse, C.; Hori, C.; Igarashi, K.; Jurgens, J. A.; Kallen, N.; Kersten, P.; Kohler, A.; Kües, U.; Kumar, T. K. A.; Kuo, A.; LaButti, K.; Larrondo, L. F.; Lindquist, E.; Ling, A.; Lombard, V.; Lucas, S.; Lundell, T.; Martin, R.; McLaughlin, D. J.; Morgenstern, I.; Morin, E.; Murat, C.; Nagy, L. G.; Nolan, M.; Ohm, R. A.; Patyshakuliyeva, A.; Rokas, A.; Ruiz-Dueñas, F. J.; Sabat, G.; Salamov, A.; Samejima, M.; Schmutz, J.; Slot, J. C.; St. John, F.; Stenlid, J.; Sun, H.; Sun, S.; Syed, K.; Tsang, A.; Wiebenga, A.; Young, D.; Pisabarro, A.; Eastwood, D. C.; Martin, F.; Cullen, D.; Grigoriev, I. V.; Hibbett, D. S. *Science* **2012**, *336*, 1715.

(7) Yakovlev, I.; Vaaje-Kolstad, G.; Hietala, A.; Stefańczyk, E.; Solheim, H.; Fossdal, C. *Appl. Microbiol. Biotechnol.* **2012**, *95*, 979.

(8) Horn, S. J.; Sørlie, M.; Vårum, K. M.; Väljamäe, P.; Eijsink, V. G. H. In *Methods in Enzymology*; Harry, J. G., Ed.; Academic Press: New York, 2012; Vol. *510*, p 69.

(9) Ray, A.; Saykhedkar, S.; Ayoubi-Canaan, P.; Hartson, S. D.; Prade, R.; Mort, A. J. *Appl. Microbiol. Biotechnol.* **2012**, *93*, 2075.

(10) Harris, P. V.; Welner, D.; McFarland, K. C.; Re, E.; Navarro Poulsen, J.-C.; Brown, K.; Salbo, R.; Ding, H.; Vlasenko, E.; Merino, S.; Xu, F.; Cherry, J.; Larsen, S.; Lo Leggio, L. *Biochemistry* **2010**, *49*, 3305.

(11) Vaaje-Kolstad, G.; Westereng, B.; Horn, S. J.; Liu, Z.; Zhai, H.; Sørlie, M.; Eijsink, V. G. H. *Science* **2010**, *330*, 219.

(12) Cantarel, B. L.; Coutinho, P. M.; Rancurel, C.; Bernard, T.; Lombard, V.; Henrissat, B. *Nucleic Acids Res.* **2009**, *37*, D233.

(13) Quinlan, R. J.; Sweeney, M. D.; Lo Leggio, L.; Otten, H.; Poulsen, J.-C. N.; Johansen, K. S.; Krogh, K. B. R. M.; Jørgensen, C. I.; Tovborg, M.; Anthonsen, A.; Tryfona, T.; Walter, C. P.; Dupree, P.; Xu, F.; Davies, G. J.; Walton, P. H. *Proc. Natl. Acad. Sci. U.S.A.* **2011**, *108*, 15079.

(14) Phillips, C. M.; Beeson, W. T.; Cate, J. H.; Marletta, M. A. *ACS Chem. Biol.* **2011**, *6*, 1399.

(15) Beeson, W. T.; Phillips, C. M.; Cate, J. H. D.; Marletta, M. A. *J. Am. Chem. Soc.* **2012**, *134*, 890.

(16) Westereng, B.; Ishida, T.; Vaaje-Kolstad, G.; Wu, M.; Eijsink, V. G. H.; Igarashi, K.; Samejima, M.; Ståhlberg, J.; Horn, S. J.; Sandgren, M. *PLoS One* **2011**, *6*, e27807.

(17) Smith, S. M.; Rawat, S.; Telser, J.; Hoffman, B. M.; Stemmler, T. L.; Rosenzweig, A. C. *Biochemistry* **2011**, *50*, 10231.

(18) Forsberg, Z.; Vaaje-Kolstad, G.; Westereng, B.; Bunæs, A. C.; Stenstrøm, Y.; MacKenzie, A.; Sørlie, M.; Horn, S. J.; Eijsink, V. G. H. *Protein Sci.* **2011**, *20*, 1479.

(19) Vaaje-Kolstad, G.; Bøhle, L. A.; Gåseidnes, S.; Dalhus, B.; Bjørås, M.; Mathiesen, G.; Eijsink, V. G. H. *J. Mol. Biol.* **2011**, *416*, 239.

(20) Aachmann, F. L.; Sørlie, M.; Skjåk-Bræk, G.; Eijsink, V. G. H.; Vaaje-Kolstad, G. *Proc. Natl. Acad. Sci. U.S.A.* **2012**, *106*, 18779.

(21) Li, X.; Beeson, W. T., IV; Phillips, C. M.; Marletta, M. A.; Cate, J. H. D. *Structure* **2012**, *20*, 1051.

(22) Bey, M.; Zhou, S.; Poidevin, L.; Henrissat, B.; Coutinho, P. M.; Berrin, J.-G.; Sigoillot, J.-C. *Appl. Environ. Microbiol.* **2013**, *79*, 488.

(23) Vaaje-Kolstad, G.; Horn, S. J.; Sørlie, M.; Eijsink, V. G. H. *FEBS J.* **2013**, epub ahead of publication, doi: 10.1111/febs.12181.

(24) Asensio, J. L.; Ardá, A.; Cañada, F. J.; Jiménez-Barbero, J. *Acc. Chem. Res.* **2012**, epub ahead of publication, doi: 10.1021/ar300024d.

(25) Langston, J. A.; Shaghasi, T.; Abbate, E.; Xu, F.; Vlasenko, E.; Sweeney, M. D. *Appl. Environ. Microbiol.* **2011**, *77*, 7007.

(26) Sygmund, C.; Kracher, D.; Scheiblbrandner, S.; Zahma, K.; Felice, A. K. G.; Harreither, W.; Kittl, R.; Ludwig, R. *Appl. Environ. Microbiol.* **2012**, *78*, 6161.

(27) Prigge, S. T.; Eipper, B. A.; Mains, R. E.; Amzel, L. M. *Science* **2004**, *304*, 864.

(28) Cramer, C. J.; Tolman, W. B. *Acc. Chem. Res.* **2007**, *40*, 601.

(29) Peisach, J.; Blumberg, W. E. *Arch. Biochem. Biophys.* **1974**, *165*, 691.

(30) Chu, H. H.; Haong, V.; Hofemeister, J.; Schrempf, H. *Microbiology* **2001**, *147*, 1793.

(31) Chmielewski, P. J. *Angew. Chem., Int. Ed.* **2010**, *49*, 1359.

(32) Saito, S.; Furukawa, K.; Osuka, A. *Angew. Chem., Int. Ed.* **2009**, *48*, 8086.

(33) Martens, C. F.; Schenning, A. P. H. J.; Feiters, M. C.; Berens, H. W.; van der Linden, J. G. M.; Admiraal, G.; Beurskens, P. T.; Kooijman, H.; Spek, A. L.; Nolte, R. J. M. *Inorg. Chem.* **1995**, *34*, 4735.

(34) Himes, R. A.; Park, G. Y.; Barry, A. N.; Blackburn, N. J.; Karlin, K. D. *J. Am. Chem. Soc.* **2007**, *129*, 5352.

(35) Kau, L. S.; Spira-Solomon, D. J.; Penner-Hahn, J. E.; Hodgson, K. O.; Solomon, E. I. *J. Am. Chem. Soc.* **1987**, *109*, 6433.

(36) Himes, R. A.; Park, G. Y.; Siluvai, G. S.; Blackburn, N. J.; Karlin, K. D. *Angew. Chem., Int. Ed.* **2008**, *47*, 9084.

(37) Fu, Y.; Tsui, H.-C. T.; Bruce, K. E.; Sham, L.-T.; Higgins, K. A.; Lisher, J. P.; Kazmierczak, K. M.; Maroney, M. J.; Dann, C. E., III; Winkler, M. E. *Nat. Chem. Biol.* **2013**, *9*, 177.

(38) Sorrell, T. N.; Malachowski, M. R. *Inorg. Chem.* **1983**, *22*, 1883.

(39) Sorrell, T. N.; Malachowski, M. R.; Jameson, D. L. *Inorg. Chem.* **1982**, *21*, 3250.

(40) Sommerhalter, M.; Lieberman, R. L.; Rosenzweig, A. C. *Inorg. Chem.* **2005**, *44*, 770.

(41) Hathaway, B. J.; Billing, D. E. *Coord. Chem. Rev.* **1970**, *5*, 143.

(42) Symons, M. C. R.; West, D. X.; Wilkinson, J. G. *J. Chem. Soc., Dalton Trans.* **1975**, 1696.

(43) Rotilio, G.; Morpurgo, L.; Giovagnoli, C.; Calabrese, L.; Mondovi, B. *Biochemistry* **1972**, *11*, 2187.

(44) Pate, J. E.; Ross, P. K.; Thamann, T. J.; Reed, C. A.; Karlin, K. D.; Sorrell, T. N.; Solomon, E. I. *J. Am. Chem. Soc.* **1989**, *111*, 5198.

(45) Boraston, A. B.; Bolam, D. N.; Gilbert, H. J.; Davies, G. J. *Biochem. J.* **2004**, *382*, 769.

(46) Schulz, M. N.; Landström, J.; Hubbard, R. E. *Anal. Biochem.* **2013**, *433*, 43.

(47) Kabsch, W. *Acta Crystallogr., Sect. D* **2010**, *66*, 125.
(48) Winn, M. D.; Ballard, C. C.; Cowtan, K. D.; Dodson, E. J.; Emsley, P.; Evans, P. R.; Keegan, R. M.; Krissinel, E. B.; Leslie, A. G.; McCoy, A.; McNicholas, S. J.; Murshudov, G. N.; Pannu, N. S.; Potterton, E. A.; Powell, H. R.; Read, R. J.; Vagin, A.; Wilson, K. S. *Acta Crystallogr., Sect. D* **2011**, *67*, 235.
(49) Vaaje-Kolstad, G.; Houston, D. R.; Riemen, A. H.; Eijsink, V. G.; van Aalten, D. M. *J. Biol. Chem.* **2005**, *280*, 11313.
(50) Stein, N. *J. Appl. Crystallogr.* **2008**, *41*, 641.
(51) McCoy, A. J.; Grosse-Kunstleve, R. W.; Storoni, L. C.; Read, R. J. *Acta Crystallogr., Sect. D* **2005**, *61*, 458.
(52) Langer, G.; Cohen, S. X.; Lamzin, V. S.; Perrakis, A. *Nat. Protoc.* **2008**, *3*, 1171.
(53) Potterton, L.; McNicholas, S.; Krissinel, E.; Gruber, J.; Cowtan, K.; Emsley, P.; Murshudov, G. N.; Cohen, S.; Perrakis, A.; Noble, M. *Acta Crystallogr., Sect. D* **2004**, *60*, 2288.
(54) Murshudov, G. N.; Vagin, A. A.; Dodson, E. J. *Acta Crystallogr., Sect. D* **1997**, *53*, 240.

■ NOTE ADDED AFTER ASAP PUBLICATION

Due to a production error, an uncorrected version of the paper was published on April 10, 2013. The corrected version was reposted on April 12, 2013.